Long-distance behaviour of the surface–atom Casimir–Polder forces out of thermal equilibrium

2006 J. Phys. A: Math. Gen. 39 6665

(http://iopscience.iop.org/0305-4470/39/21/S67)

INSTITUTE OF PHYSICS PUBLISHING JOURNAL OF PHYSICS A: MATHEMATICAL AND GENERAL

J. Phys. A: Math. Gen. **39** (2006) 6665–6677 doi:10.1088/0305-4470/39/21/S67

Long-distance behaviour of the surface–atom Casimir–Polder forces out of thermal equilibrium

L P Pitaevskii

Dipartimento di Fisica, Università di Trento and Centro di recerca e svilupo BEC, INFM-CNR, Via Sommarive 14, I-38050 Povo, Trento, Italy
and
Kapitza Institute for Physical Problems, ul. Kosygina 2, 119334 Moscow, Russia

E-mail: lev@science.unitn.it

Received 7 November 2005, in final form 3 January 2006
Published 10 May 2006
Online at stacks.iop.org/JPhysA/39/6665

Abstract

Long-distance behaviour of the Casimir–Polder–Lifshitz force between an atom and the surface of a substrate is investigated. When the temperatures of the substrate and the environment are different, the new decay law $1/z^3$ of the force at large distances is discovered, which is slower than at thermal equilibrium. The force is of a quantum nature and attractive or repulsive depending on whether the temperature of the substrate is higher or lower than that of the environment. A transparent derivation of this law is presented. It is based on a picture of evanescent waves, created in vacuum by the black-body radiation impinging on the surface near the angle of total reflection. Some new experimental possibilities of the measurement of the forces are discussed: oscillations of a Bose–Einstein condensate near the surface, Bloch oscillations of fermions in an optical lattice and phase evolution of a BEC in a double-well trap.

PACS numbers: 34.50.Dy, 42.50.Vk, 39.20.+q, 03.75.Kk

(Some figures in this article are in colour only in the electronic version)

1. Introduction: surface–atom forces in equilibrium

The study of the force felt by an atom near a surface has recently become a popular subject of research (see, for example, [1, 2] and references therein). These studies are motivated both by the possibility of nanotechnological applications [3] as well as by the search for stronger constraints on hypothetical non-Newtonian forces [4, 5]. Experimental and theoretical research has recently been focused on the forces acting on ultracold atomic gases, including atomic beams [6–9], Bose–Einstein condensates [2, 10–12] and degenerate Fermi gases [13].

At thermal equilibrium the force can be presented in the form

$$F^{\rm eq}(T,z) = F_0(z) + F^{\rm eq}_{\rm th}(T,z) \tag{1}$$

where we have separated the contribution $F_0(z)$ arising from the $T = 0$ zero-point fluctuations and the one arising from the thermal fluctuations. At short distances z (typically less than fractions of microns), the zero-point component behaves like $1/z^4$ and is the analogue of the van der Waals–London interatomic force. At larger distances, the relativistic retardation effects give rise to a different $1/z^5$ dependence characterizing the so-called Casimir–Polder regime [14, 15]:

$$F_0(z)_{z\to\infty} = -\frac{3}{2}\frac{\hbar c\alpha_0}{\pi z^5}\frac{\varepsilon_0 - 1}{\varepsilon_0 + 1}\phi(\varepsilon_0). \tag{2}$$

(For definition of the function $\phi(\varepsilon_0)$ see [2].)

The second component of the force is due to the thermal fluctuations of the electromagnetic field. This effect was first considered by Lifshitz [16]. We will refer to it as to the Lifshitz force. At distances larger than the thermal photon wavelength $\lambda_T = \hbar c/T$ (corresponding to $\sim$7.6 μm at room temperature) this force decays, at thermal equilibrium, like $1/z^4$ (we use units with $k_{\rm B} = 1$):

$$F^{\rm eq}_{\rm th}(T,z)_{z\to\infty} = -\frac{3}{4}\frac{T\alpha_0}{z^4}\frac{\varepsilon_0 - 1}{\varepsilon_0 + 1}. \tag{3}$$

The explicit behaviour of the force (1) at all distances has been recently investigated in [2].

The asymptotic law (3) is reached at distances larger than the thermal wavelength λ_T. In the above equations, α_0 (=47.3 $\times$ 10^{-24} cm^3 for Rb atoms) and ε_0 are, respectively, the static polarizability of the atom and the static dielectric function of the substrate. It is worth noting that only the static optical properties enter the asymptotic laws (2) and (3), the corresponding dynamic effects becoming important only at shorter distances. It is also worth noting that the asymptotic behaviour of the thermal force has a classical nature, being independent of the Planck constant. In the present paper, we are interested in the thermal component of the force. The Lifshitz force was originally evaluated at full thermodynamic equilibrium. A non-trivial problem is the study of the force out of thermal equilibrium, when the temperatures of the substrate and of the surrounding walls located at large distances (hereafter called environment temperature) do not coincide. The problem is important both from an experimental point of view, due to the possibility of tuning the two temperatures independently, and for a better understanding of the interplay between zero-point and thermal-fluctuation effects. A first important investigation of the surface–atom force out of thermal equilibrium was carried out by Henkel *et al* [17] who calculated the force, assuming that the dielectric substrate is at finite temperature while the environment temperature is zero, and investigated the behaviour of the force at short distances. It has been shown in [18] that, out of thermal equilibrium, the force acting on the atom exhibits a new asymptotic behaviour, characterized by a $1/z^3$ decay at large distances.

2. Non-equilibrium surface–atom forces

The purpose of the present paper is to discuss the calculation of the non-equilibrium forces and in particular to investigate its behaviour at large distances. The theory which we develop is a generalization of the equilibrium Lifshitz theory. In this theory, a fluctuating electromagnetic field is created by sources—fluctuating polarization of the media. Correlation functions of the Fourier components of quantum operators of these fluctuating dipole moments are, according

to the fluctuation–dissipation theorem,

$$\frac{1}{2}\left\langle \hat{P}_i^{\mathrm{fl}}(\boldsymbol{r},\omega)\,\hat{P}_k^{\mathrm{fl}}(\boldsymbol{r}',\omega') + \hat{P}_k^{\mathrm{fl}}(\boldsymbol{r}',\omega')\,\hat{P}_i^{\mathrm{fl}}(\boldsymbol{r},\omega)\right\rangle = \frac{1}{2\pi}\hbar\varepsilon''(\boldsymbol{r},\omega)\left(\frac{1}{2}+\frac{1}{\mathrm{e}^{\hbar\omega/T}-1}\right)\delta(\omega+\omega')\delta_{ik}\delta(\boldsymbol{r}-\boldsymbol{r}'). \tag{4}$$

Transition to the particular case of a transparent medium must be produced in this theory by the limiting procedure $\varepsilon'' \to 0$ in the final solution. For the first time equation (4) was obtained by Rytov [19]. He assumed the δ-correlations of sources and matched the coefficient to obtain correct formulae for black-body radiation outside the bodies. Landau and Lifshitz derived (4) using the fluctuation–dissipation theorem [20].

Due to the presence of the $\delta(\boldsymbol{r}-\boldsymbol{r}')$ factor these fluctuations are *local*. Fluctuations of the sources at different points of the material are non-coherent. This permits us to assume that in the non-equilibrium situation, when temperature T is different at different points, in our case in two half-spaces, the sources' correlations are given by the same equations. I must emphasize that this assumption, even being quite reasonable, is still a hypothesis, which is useful for both further theoretical investigation and experimental verification.

Polder and Van Hove calculated, using this approach, the radiative heat transfer between two bodies with different temperatures [21].

Let us consider an atom with dielectric polarizability $\alpha(\omega)$ placed in vacuum at distance z from the flat surface of a substrate made of a material with dielectric function $\varepsilon(\omega) = \varepsilon'(\omega) + \mathrm{i}\varepsilon''(\omega)$. We choose a coordinate system with the xy plane coinciding with the interface and the z-axis such that the substrate occupies the region with $z < 0$ and the vacuum the region with $z > 0$. We also assume that the substrate is locally at thermal equilibrium at a temperature T_{S} which can differ from the environment temperature T_{E}, the global system being out of thermal equilibrium, but in a stationary state. The total electromagnetic field will be in general the sum of the radiation produced by the substrate and the one of the environment. The latter radiation will be partially absorbed and reflected from the substrate. In typical experiments with ultracold atomic gases, the environment temperature is determined by the chamber containing the substrate and the trapped atoms. We again present the force as the sum of the zero-temperature contribution $F_0(z)$ and of a thermal contribution which, however, is different from $F_{\mathrm{th}}^{\mathrm{eq}}$ if $T_{\mathrm{S}} \neq T_{\mathrm{E}}$:

$$F^{\mathrm{neq}}(T_{\mathrm{S}}, T_{\mathrm{E}}, z) = F_0(z) + F_{\mathrm{th}}^{\mathrm{neq}}(T_{\mathrm{S}}, T_{\mathrm{E}}, z). \tag{5}$$

We introduce now the main assumption of the theory. We will treat the atoms as being at zero temperature in the sense that the surrounding radiation is not able to populate their excited states which are assumed to be located at energies $\hbar\omega_{\mathrm{at}}$ much higher than the thermal energy:

$$T_{\mathrm{S}}, T_{\mathrm{E}} \ll \hbar\omega_{\mathrm{at}}. \tag{6}$$

This condition is very well satisfied at ordinary temperatures. For example, the first optical resonance of Rb atoms corresponds to 1.8×10^4 K.[1] It is worth noting that at $T \sim \hbar\omega_{\mathrm{at}}$ the majority of atoms would be ionized.

Inequality (6) results in important simplifications. First of all, this means that we can substitute the atomic dielectric polarizability $\alpha(\omega)$ with its real static value $\alpha(0) \equiv \alpha_0$ in all equations related to the thermal radiation. Further we can neglect thermal fluctuations of the

[1] Ground-state energy levels of alkali atoms are split into hyperfine components and, in the presence of a magnetic field, into Zeeman components. Electric dipole transitions between these levels are forbidden and they are not important for optical properties. However, their role is worth more careful investigation. The contribution to the force due to the magnetic dipole transitions between such levels was estimated for $T = 0$ in [22].

dipole moment of the atom, because according to (4) these fluctuations are created by the imaginary part of polarizability α''. In these conditions, the thermal part of the force, acting on the atom, can be presented in the form

$$F_{\rm th}^{\rm neq}(T,0,z) = 4\pi\alpha_0\partial_z U_{\rm El} \tag{7}$$

where $U_{\rm El} = \langle E^2\rangle/8\pi$ is the thermal component of the electric energy density in vacuum, calculated in the absence of the atom. Note that the force (7) is entirely similar to the dipole force acting on an atom in the presence of an inhomogeneous laser field.

We can now discuss the behaviour of the force when the system is not in equilibrium. It is enough to consider the case of a substrate at finite temperature ($T_{\rm S} = T \neq 0$) in the absence of the environment radiation ($T_{\rm E} = 0$). In order to discuss the general case $T_{\rm S} \neq T_{\rm E} \neq 0$, we can use the additivity property of the thermal force which can be written, in general, as the sum of two contributions:

$$F_{\rm th}^{\rm neq}(T_{\rm S}, T_{\rm E}, z) = F_{\rm th}^{\rm neq}(T_{\rm S}, 0, z) + F_{\rm th}^{\rm neq}(0, T_{\rm E}, z), \tag{8}$$

produced, respectively, by the radiation of the substrate and of the environment. Equation (8) immediately follows from the locality of the radiation sources (4) and linearity of the Maxwell equations. The full surface–atom force out of equilibrium can be finally written in the convenient form

$$F^{\rm neq}(T_{\rm S}, T_{\rm E}, z) = F^{\rm eq}(T_{\rm E}, z) + F_{\rm th}^{\rm neq}(T_{\rm S}, 0, z) - F_{\rm th}^{\rm neq}(T_{\rm E}, 0, z) \tag{9}$$

where the equilibrium force $F^{\rm eq}(T, z)$ is given by (1).

To calculate the force (7), one must solve the Maxwell equations for electric field in terms of P_i using corresponding Green's function and perform averaging of E^2 with the help of (4). This problem was solved by Henkel *et al* [17] who obtained the result

$$F_{\rm th}^{\rm neq}(T,0,z) = \frac{\hbar}{2\pi^2}\alpha_0\int_0^\infty {\rm d}\omega\frac{\varepsilon''(\omega)}{{\rm e}^{\hbar\omega/T}-1}{\rm Re}\left[\int_{V_{\rm S}} G_{ik}[\omega;\boldsymbol{r},\boldsymbol{r}_1]\partial_z G_{ik}^*[\omega;\boldsymbol{r},\boldsymbol{r}_1]\,{\rm d}^3\boldsymbol{r}_1\right] \tag{10}$$

for the thermal contribution to the force[2]. In (10), G_{ik} is the retarded Green's function of the electromagnetic field. The variable $\boldsymbol{r}_1$ should be integrated on the volume $V_{\rm S}$ occupied by the substrate which provides the source of the thermal radiation. The argument $\boldsymbol{r}$ defines the position of the atom outside the substrate.

Explicit calculation of (10) demands lengthy algebra. It can be performed by introducing the Fourier transform $g_{ik}[\omega;\boldsymbol{k}_\perp, z_a, z_b]$ of the Green's function $G_{ik}[\omega;\boldsymbol{r}_a,\boldsymbol{r}_b]$ where $\boldsymbol{k}_\perp$ is the component of the electromagnetic wave vector parallel to the interface. The detail of calculations will be published elsewhere. I do not reproduce here the final equation for the force (10), see equation (8) in [18] and Antezza's contribution in this volume. Instead I will discuss the large z behaviour of the out of equilibrium force. The most striking result of the non-equilibrium theory is that this behaviour is completely different from the equilibrium case. As shown in [18], the force (10) exhibits the non-trivial asymptotic behaviour

$$F_{\rm th}^{\rm neq}(T,0,z)_{z\to\infty} = -\frac{\hbar\alpha_0}{z^3\pi c}\int_0^\infty {\rm d}\omega\frac{\omega}{{\rm e}^{\hbar\omega/T}-1}f(\omega). \tag{11}$$

Thus the force exhibits a slower $1/z^3$ decay with respect to the one holding at thermal equilibrium where it decays like $1/z^4$ (see (3)). In the above equation, we have introduced the function

$$f(\omega) = (|\varepsilon(\omega)-1| + (\varepsilon'(\omega)-1))^{\frac{1}{2}}\frac{2+|\varepsilon(\omega)-1|}{\sqrt{2}|\varepsilon(\omega)-1|} \tag{12}$$

[2] In the general case, the thermal force also contains a repulsive coordinate-independent *wind* part proportional to $\alpha''(\omega)$ and produced by the absorption of photons by the atom. Due to condition (6), this wind contribution can be ignored.

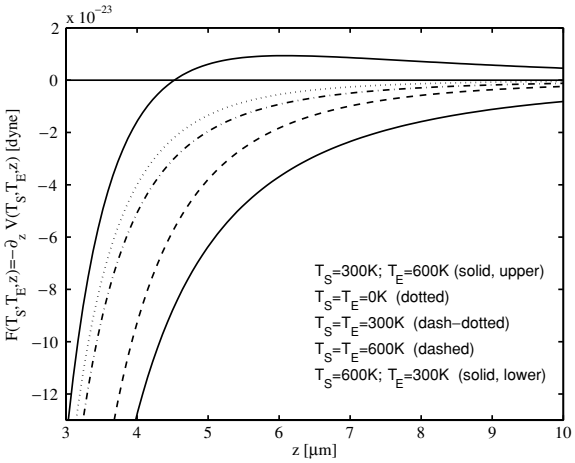

Figure 1. Surface–atom force $F^{\rm neq}(z)$, calculated from (9), for different temperatures of the substrate and the environment. From [18].

which depends on the optical properties of the substrate. For temperatures much smaller than the energy $\hbar\omega_c$, where ω_c is the lowest characteristic frequency of the dielectric substrate, we can replace $f(\omega)$ with its low-frequency limit $(\varepsilon_0+1)/\sqrt{\varepsilon_0-1}$. The force felt by the atom then approaches the asymptotic limit

$$F^{\rm neq}(T,0,z)_{z\to\infty} = -\frac{\pi}{6}\frac{\alpha_0 T^2}{z^3 c\hbar}\frac{\varepsilon_0+1}{\sqrt{\varepsilon_0-1}}, \tag{13}$$

holding at low temperature and at distances $z \gg \lambda_{\rm T}/\sqrt{\varepsilon_0-1}$, where $\lambda_{\rm T}$ is the thermal photon wavelength. This condition demands larger z for small ε_0-1. In contrast, in the limit $\varepsilon_0\to 1$ at fixed z the force tends to zero as it must. Note that $\varepsilon_0 = 9.4$ and 3.83 for the sapphire and silica substrates correspondingly.

Using (9) one can easily generalize equation (13) for the case when the environment has the finite temperature $T_{\rm E}$. Indeed, at $z\to\infty$ the first term in (9) is small in comparison to the other and we obtain

$$F^{\rm neq}(T_{\rm S},T_{\rm E},z)_{z\to\infty} = -\frac{\pi}{6}\frac{\alpha_0\left(T_{\rm S}^2-T_{\rm E}^2\right)}{z^3 c\hbar}\frac{\varepsilon_0+1}{\sqrt{\varepsilon_0-1}}. \tag{14}$$

Equation (14) shows that, at large distances, the new force is attractive or repulsive depending on whether the substrate temperature is higher or smaller than the environment one. Furthermore, it exhibits a stronger temperature dependence with respect to equilibrium and explicitly contains the Planck constant.

In figure 1 we show the results for the force obtained starting from (10) as a function of the distance from the surface for different choices of $T_{\rm S}$ and $T_{\rm E}$. Calculations have been done for a sapphire substrate and for rubidium atoms. For $F^{\rm eq}(T,z)$, we have used the predictions of [2]. The figure clearly shows that the thermal effects out of equilibrium (solid lines) are sizable , thereby providing promising perspectives for future measurements of the surface–atom force at large distances. In particular, in order to increase the attractive nature of the force it is much more convenient to heat the substrate by keeping the environment at room temperature (lower solid line) rather than heating the whole system (dashed line). When $T_{\rm S} < T_{\rm E}$ (upper solid line), the force exhibits a characteristic change of sign reflecting a repulsive nature at large distances in accordance with (14). We have presented the results for the force. However, it is useful to also calculate the potential and the gradient of the force

because the corresponding predictions can be of interest for different types of experiments with ultracold gases. Experiments based on the study of the centre of mass oscillation of a trapped gas are sensitive to the gradient of the force [2]. The corresponding frequency shifts produced by the surface–atom interaction have been recently measured [12] in conditions of thermal equilibrium in agreement with the predictions of theory [2]. Conversely, experiments based on Bloch oscillations are sensitive to the force itself [23, 13]. Finally, one can also think of interference experiments with Bose–Einstein condensates in a double-well potential. For large separations between the wells, the positions of the corresponding interference fringes are sensitive to the potential [24]. We will discuss some details of corresponding experiments in section 4.

Equation (14) holds for a dielectric substrate where ε_0 is finite. For a metal, if one uses the Drude model, one has $\varepsilon''(\omega) = 4\pi\sigma/\omega$ with the real part $\varepsilon'(\omega)$ remaining finite as $\omega \to 0$ so that one finds $f(\omega) \to \sqrt{\varepsilon''(\omega)/2} = \sqrt{2\pi\sigma/\omega}$. At low temperatures, one obtains then a different temperature dependence

$$F^{\mathrm{neq}}(T_{\mathrm{S}}, T_{\mathrm{E}}, z)_{z\to\infty} = -\frac{\alpha_0\zeta(3/2)\sqrt{\sigma}\left(T_{\mathrm{S}}^{3/2} - T_{\mathrm{E}}^{3/2}\right)}{z^3 c\sqrt{2\hbar}} \tag{15}$$

where $\zeta(3/2) \approx 2.61$ is the Riemann function. Note that from this point of view the Lifshitz $1/z^4$ asymptotic (3) is a result of a non-trivial cancellation of the non-equilibrium $1/z^3$ terms.

3. Direct derivation of the non-equilibrium asymptotic law

In this section, I will give a simple and transparent derivation of the non-equilibrium asymptotic law (13). I hope that this derivation helps to understand the physical meaning of the non-trivial asymptotic behaviour of the non-equilibrium force. Of course, this derivation cannot substitute the full theory presented in the previous section. We assume from the very beginning that one can neglect *absorption* and dispersion of the dielectric function of the substrate (and, of course, of the atom polarizability) and consider the asymptotic limit $z \to \infty$. The derivation is based on the next three obvious observations:

1. In the case of the zero-temperature environment and in the absence of absorption in the substrate, the thermal radiation is the black-body radiation, which comes from $z = -\infty$. The radiation cannot be created on finite distances because there is no absorption and cannot come from $z = +\infty$ because the half-space $z > 0$ is cold.

2. The force can be created only by the *evanescent* waves, whose amplitude decreases when $z \to +\infty$. Hence only the radiation, which *undergoes the total reflection*, contributes to the force. (Propagating waves create the 'energy wind', which does not contribute to the force in the absence of absorption by the atom.)

3. However, asymptotically the incident waves are most important, which come *nearly at the angle θ_r of the total reflection,* $\sin\theta_r = 1/\sqrt{\varepsilon_0}$. These waves decay slowly at positive z.

At $z < 0$, one has the incident wave

$$\boldsymbol{E}_0 = \mathrm{Re}\,\hat{\boldsymbol{E}}_0\,\mathrm{e}^{\mathrm{i}(\boldsymbol{k}_0\cdot\boldsymbol{r}-\omega t)}. \tag{16}$$

(In this section, quantities with 'hats' ˆ are the complex amplitudes of fields.) One has

$$\boldsymbol{k}_0=\{\boldsymbol{k}_\perp, k_{0z}\}; \qquad k_0^2 = \omega^2\varepsilon_0/c^2, \qquad k_{0z} = \sqrt{\omega^2\varepsilon_0/c^2 - k_\perp^2} \tag{17}$$

where $k_\perp$ is the projection of the wave vector on the substrate surface and ε_0 is, as before, the static dielectric function of the substrate. According to the observation 2, we must consider only the case of total reflection. Correspondingly, we assume that $\omega\sqrt{\varepsilon_0}/c > k_\perp > \omega/c$. There is also the reflected wave $\boldsymbol{E}_1 = \mathrm{Re}\,\hat{\boldsymbol{E}}_1\exp(\mathrm{i}(\boldsymbol{k}_\perp\cdot\boldsymbol{r}_\perp - zk_{0z} - \omega t))$. At $z > 0$, one has

the refracted wave $\boldsymbol{E} = \mathrm{Re}\,\hat{\boldsymbol{E}}\exp(\mathrm{i}(\boldsymbol{k}_\perp\cdot\boldsymbol{r}_\perp-\omega t))\,\mathrm{e}^{\mathrm{i}zk_z}$. We consider only the *evanescent* refracted waves with $k_z = \mathrm{i}\kappa$:

$$\boldsymbol{E} = \mathrm{e}^{-\kappa z}\,\mathrm{Re}\,\hat{\boldsymbol{E}}\exp(\mathrm{i}(\boldsymbol{k}_\perp\cdot\boldsymbol{r}_\perp-\omega t)), \qquad \kappa = \sqrt{k_\perp^2-\omega^2/c^2}. \tag{18}$$

The angle of total reflection corresponds to $\kappa = 0$, i.e., $k_{0z} = \omega\sqrt{\varepsilon_0-1}/c$. Actually, we must keep $\kappa \neq 0$ only in the exponential factor (18).

One can establish relations between $\hat{\boldsymbol{E}}_0$ and $\hat{\boldsymbol{E}}$ using the textbook Fresnel equations. The relations are different for different polarizations of the fields.

Case I: TE waves. Electric field $\boldsymbol{E}$ is perpendicular to the plane of incidence. One can use general equations from the textbook [20], section 66. Equation (66.4) gives for the refracted field amplitudes:

$$\hat{E}_{\mathrm{TE}} = \frac{2k_{0z}}{k_{0z}+k_z}\hat{E}_{0\mathrm{TE}} = \frac{2k_{0z}}{k_{0z}+\mathrm{i}\kappa}\hat{E}_{0\mathrm{TE}}. \tag{19}$$

At the angle of total reflection, i.e., at $\kappa \to 0$, we have simply $\hat{E}_{\mathrm{TE}} = 2\hat{E}_{0\mathrm{TE}}$. This gives the relation between squares of fields (averaged with respect to time):

$$E^2_{\mathrm{TE}} = \tfrac{1}{2}|\hat{E}_{\mathrm{TE}}|^2\,\mathrm{e}^{-2\kappa z} = 4E^2_{0\mathrm{TE}}\,\mathrm{e}^{-2\kappa z}. \tag{20}$$

Case II: TM waves. Magnetic field $\boldsymbol{H}$ is perpendicular to the plane of incidence. Equation (66.6) from [20] gives instead (19) $\hat{H}_{\mathrm{TM}} = \frac{2k_{0z}}{k_{0z}+\varepsilon_0 k_z}\hat{H}_{0\mathrm{TM}} \approx 2\hat{H}_{0\mathrm{TM}}$ or $H^2_{\mathrm{TM}} = 4H^2_{0\mathrm{TM}}\,\mathrm{e}^{-2\kappa z}$. According to the properties of plane waves[3]:

$$H^2_{\mathrm{TM}} = E^2_{\mathrm{TM}}, \qquad H^2_{0\mathrm{TM}} = \varepsilon_0 E^2_{0\mathrm{TM}}. \tag{21}$$

Thus, we have in the TM case

$$E^2_{\mathrm{TM}} = 4\varepsilon_0 E^2_{0\mathrm{TM}}\,\mathrm{e}^{-2\kappa z}. \tag{22}$$

Now we can calculate the thermal average of E^2_{TE} and E^2_{TM}, taking into account that $\boldsymbol{E}_0$ is the field of the black-body radiation. Energy of the black-body radiation in the interval of wave vectors $\mathrm{d}\boldsymbol{k}_0$ is

$$U^{\mathrm{BB}}_{\mathrm{d}\boldsymbol{k}_0} = 2\times\frac{\varepsilon_0\langle E^2_0\rangle_{\mathrm{d}\boldsymbol{k}_0}}{8\pi} = \frac{\hbar\omega}{\mathrm{e}^{\hbar\omega/T}-1}\frac{2\,\mathrm{d}\boldsymbol{k}_0}{(2\pi)^3}, \tag{23}$$

where the factor 2 is due to the presence of the magnetic energy and both polarizations give the same contributions $\langle E^2_{0\mathrm{TE}}\rangle_{\mathrm{d}\boldsymbol{k}_0} = \langle E^2_{0\mathrm{TM}}\rangle_{\mathrm{d}\boldsymbol{k}_0} = \langle E^2_0\rangle_{\mathrm{d}\boldsymbol{k}_0}/2$. This means that one can perform averaging by substituting

$$E^2_{0\mathrm{TE}},\, E^2_{0\mathrm{TM}} \to \frac{2\pi}{\varepsilon_0}\frac{\hbar\omega}{\mathrm{e}^{\hbar\omega/T}-1}\frac{2\,\mathrm{d}\boldsymbol{k}_0}{(2\pi)^3} \tag{24}$$

into equations (20) and (22) and integrating over the total reflection region. This gives

$$\frac{\langle E^2_{\mathrm{TM}}\rangle}{8\pi} = \varepsilon_0\frac{\langle E^2_{\mathrm{TE}}\rangle}{8\pi} = 2\int_{k_\perp>\omega/c}\mathrm{e}^{-2\kappa z}\frac{\hbar\omega}{\mathrm{e}^{\hbar\omega/T}-1}\frac{\mathrm{d}\boldsymbol{k}_0}{(2\pi)^3}. \tag{25}$$

Thus, the density of the energy of the electric field in vacuum $U_{\mathrm{El}} \equiv \langle E^2\rangle/8\pi = \langle E^2_{\mathrm{TE}}+E^2_{\mathrm{TM}}\rangle/8\pi$ is

$$U_{\mathrm{El}} = \frac{\varepsilon_0+1}{\varepsilon_0}\int_{k_\perp=\omega/c}^{k_\perp=\omega\sqrt{\varepsilon_0}/c}\mathrm{e}^{-2\kappa z}\frac{\hbar\omega}{\mathrm{e}^{\hbar\omega/T}-1}\frac{2\,\mathrm{d}\boldsymbol{k}_0}{(2\pi)^3}. \tag{26}$$

[3] The first equation (21) is valid for the propagating plane waves. The corresponding equation for the evanescent waves is $(1+2\kappa^2c^2/\omega^2)H^2_{\mathrm{TM}} = E^2_{\mathrm{TM}}$. It is reduced to (21) at $\kappa \to 0$.

The element $\mathrm{d}\boldsymbol{k}_0$ can be written in the cylindrical coordinates as $\mathrm{d}\boldsymbol{k}_0 = 2\pi k_\perp \mathrm{d}k_\perp\, \mathrm{d}k_{0z}$. Then, taking into account that $k_\perp^2 = \kappa^2 + \omega^2/c^2$, we have

$$\mathrm{d}k_{0z} = \frac{\varepsilon_0 \omega\, \mathrm{d}\omega}{c^2 k_{0z}} \approx \frac{\varepsilon_0\, \mathrm{d}\omega}{c\sqrt{\varepsilon_0 - 1}}, \qquad k_\perp \mathrm{d}k_\perp = \kappa\, \mathrm{d}\kappa, \qquad \mathrm{d}\boldsymbol{k}_0 = 2\pi \frac{\varepsilon_0\, \mathrm{d}\omega\, \kappa\, \mathrm{d}\kappa}{c\sqrt{\varepsilon_0 - 1}} \tag{27}$$

because for small κ we can change in the denominator $k_{0z} \approx \omega\sqrt{\varepsilon_0 - 1}/c$. Equation (26) takes the form

$$\frac{\langle E^2 \rangle}{8\pi} = \frac{\varepsilon_0 + 1}{\sqrt{\varepsilon_0 - 1}} \frac{1}{2\pi^2 c^3} \int_0^\infty \frac{\hbar\omega}{\mathrm{e}^{\hbar\omega/T} - 1} \int_0^{(\sqrt{\varepsilon_0 - 1})\omega/c} \mathrm{e}^{-2z\kappa} \kappa\, \mathrm{d}\kappa\, \mathrm{d}\omega. \tag{28}$$

At $z \to \infty$, only small values of $\kappa \sim 1/z$ are important. Thus, if

$$z \gg c/(\omega\sqrt{\varepsilon_0 - 1}) \sim \hbar c/(T\sqrt{\varepsilon_0 - 1}) \tag{29}$$

we can integrate with respect to κ from 0 to ∞. Finally, the integrations give

$$U_{\mathrm{El}} = \frac{\langle E^2 \rangle}{8\pi} = \frac{1}{48} \frac{\varepsilon_0 + 1}{z^2\sqrt{\varepsilon_0 - 1}} \frac{T^2}{c\hbar}. \tag{30}$$

Using equation (7) for the force in terms of $\partial_z U_{\mathrm{El}}$, we recover (13).

The dependence of the electric energy U_{El} on temperature and distance can be physically understood by noting that, as is obvious from (27) and (28), the main contribution to the zth-dependent part of U_{El} arises from the black-body radiation impinging on the surface in a small interval of angles, of the order of $(\lambda_T/z)^2$, near the angle of total reflection. This radiation creates slowly damping evanescent waves in vacuum. This means that the energy of the electric field in the vacuum U_{El} is of the order of $(c^2\hbar^2/T^2z^2)U^{\mathrm{BB}}$, where $U^{\mathrm{BB}} \propto T^4$ is the density of energy of the black-body radiation, in accordance with (30). As a result, $F^{\mathrm{neq}}(T, 0, z)$ turns out to be, in accordance with (13), of the order of $\left(\lambda_T^2/z^3\right)U^{\mathrm{BB}}$. Note that in the equilibrium case, when the temperature of the environment is equal to the temperature of the substrate, the asymptotic term (30) is cancelled by the contribution of the radiation from the environment. At condition (29), the waves incident on the surface under the grazing angles are important.

4. Experiments with trapped ultracold gases: new possibilities

In this section, we give a short review of some new experimental devices which have been used or can be used for measurements of the atom–surface forces.

4.1. Oscillations of a Bose–Einstein condensate near a surface

For the first time oscillations of a BEC were used to measure forces between atoms and a surface in [11].

Systematic investigation of the forces between atoms and substrate was performed in [12]. The scheme of the experiment is shown in the upper part of figure 2. A cigar-shaped condensate, containing 1.4×10^5 of ^{87}Rb atoms in $|F = 1, m_F = -1\rangle$ ground state, was trapped in a magnetic trap with frequencies $\omega_z = 6.4$ Hz in the axial direction and $\omega_x = \omega_y = 228$ Hz in the radial directions. The Thomas–Fermi radius was about 2.4 μm. The condensate was placed near the fused silica surface with z-axis parallel to the surface and x-axis in the direction of the gravity force. The presence of the Casimir force F resulted in the frequency shift, which for a thin condensate can be calculated as

$$\gamma_x \equiv \frac{\omega_x - \omega_x'}{\omega_x} \simeq \frac{1}{2\omega_x^2 m} \partial_x F. \tag{31}$$

In real conditions, the gradient of the force must be averaged over the condensate size [2].

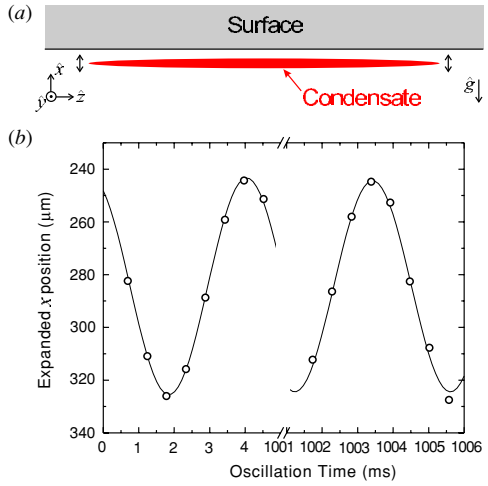

Figure 2. Measurement of the forces using dipole oscillations of a condensate. (*a*) Aspect ratio of the condensate and its position relative to the surface. (*b*) Typical data showing the condensate positions after expansions. From [12].

The distance between the condensate and the surface was measured by an absorption imaging technique. The atoms were illuminated with a beam perpendicular to the long axis of the condensate. This beam impinges on the surface with a slight grazing incidence angle of $\sim 2.4^\circ$ such that when the condensate is within ~ 100 μm of the surface, both a direct absorption image and a reflected absorption image of the condensate appear. Measuring the distance between these images allows us to determine the distance between the condensate and the surface.

The typical experiment was performed as follows. To excite a condensate dipole oscillation, a pulse of an oscillating magnetic field was applied with the frequency near the radial trap frequency. After some 'waiting time', the atoms were transferred by a microwave field into the $|F = 2, m_F = -2\rangle$ state, which is antitrapped, i.e., atoms in this state were pushed away from the magnetic field minimum. As a result of the action of the gravitational field and the antitrapping, the condensate dropped from the surface and expanded. After 5 ms of this expansion the position of the condensate was imaged through absorption. Repeating this procedure with different waiting times permits us to reconstruct the oscillations. The antitrapped expansion acts to amplify the oscillation amplitude by approximately 20-fold, permitting straightforward measurement of the oscillation in expansion (see figure 2(*b*)).

The results of the measurement of the Casimir–Polder force from the surface are shown in figure 3. One can see good agreement with the predicted Casimir–Polder force from a fused silica surface, but not with the extrapolation of the van der Waals–London force. Unfortunately, it was impossible in these experiments to have the experimental resolution to discern between the $T = 0$ K Casimir–Polder force and the $T = 300$ K case. Looking for the thermal effects at an elevated temperature, however, appears promising; see figure 3 for the prediction for $T = 600$ K. At this temperature, the predicted γ_x is larger than nearly all of data. Thus, a measurement at this temperature should yield a significantly larger signal. The effect can be increased even more in non-equilibrium conditions, if only the substrate is heated, as discussed in section 2.

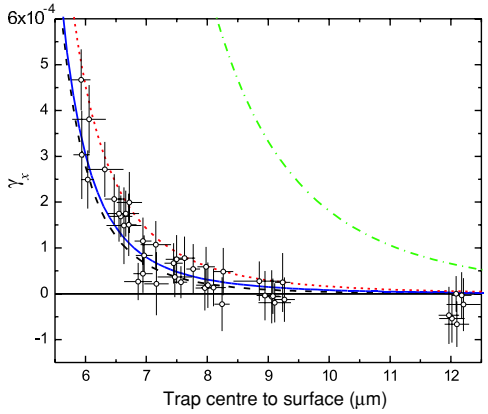

Figure 3. Frequency shift γ_x from the fused silica surface. Theoretical predictions of the theory [2] are shown for $T = 0$ K (dashed line), $T = 300$ K (solid line) and $T = 600$ K (dotted line). The dash–dotted line is the extrapolation of the van der Waals–London $1/d^3$ potential. From [12].

Figure 4. Schematic diagram of the set-up for the measurement of the Casimir–Polder forces using Bloch oscillations. From [13].

4.2. Measurement of small forces using Bloch oscillations

In the experiments described in the previous subsection, the Casimir forces were measured using oscillations of atoms near the surface in real, coordinate space. Here, we will discuss the possibility of sensitive measuring of forces by observation oscillations in momentum space, namely, the Bloch oscillations of atoms in a periodical optical lattice. The scheme of the experiments is presented in figure 4. A sample of ultracold atoms is trapped in a 1D optical lattice aligned with gravity. A vertical harmonic potential is presented and horizontal confinement is provided by the same laser beam as the lattice. As soon as the vertical confinement is switched off, the atoms start to perform the Bloch oscillation in the lattice under the action of gravity. The quasi-momentum q evolves according to the equation $\hbar\, \mathrm{d}q/\mathrm{d}t = mg$ or $q = mgt/\hbar$. However, all observable physical quantities, the momentum distribution in particular, are periodic functions of q with the period equal to $2\pi/\lambda$ (λ is the wavelength of the lattice). As a result, the momentum distribution oscillates with a well-defined period

$$T_B = \frac{2\pi\hbar}{mg\lambda}. \tag{32}$$

The Bloch oscillations decay due to different processes, related to interaction between atoms. This interaction, however, is very small for spin-polarized cold fermions. In experiments [23] with atoms of ^{40}K more than 100 periods of oscillations have been observed.

To measure momentum distribution, the atomic cloud was released from the lattice at a given time. After 8 ms ballistic expansion, the spatial distribution of the cloud density was measured by absorption imaging. This density distribution directly gives the momentum

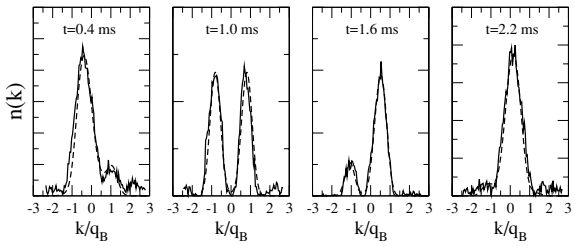

Figure 5. Momentum distribution of a Fermi gas performing Bloch oscillations in the gravitational field for different times. Solid lines are experimental data and dashed lines are theoretical calculations. From [13].

distribution at the beginning of the expansion. The evolution of the momentum distribution is shown in figure 5. One can see the change from the initial monotonic distribution to the characteristic two-peaks distribution at $t = T_B/2$. Observation of many periods of oscillations permits us to define the period with very high accuracy. As an example, the gravitational force g was measured with five-digit accuracy [23].

To measure Casimir forces, one must bring a surface close to the atomic cloud. Then the Casimir–Polder force F will shift the Bloch oscillation period. The shift in the first approximation with respect to F is

$$\frac{\Delta T_B}{T_B} = -\frac{\bar{F}}{mg} \tag{33}$$

where $\bar{F}$ is the Casimir–Polder force, properly averaged over the volume of the cloud. Thus, the force itself will be measured in these experiments, not the gradient of force as in [12]. The effect will be of the order of 10^{-4}–10^{-5}, while one can expect to obtain an overall sensitivity $\Delta T_B/T_B = 10^{-6}$–10^{-7} [13].

To obtain a good spatial resolution, it is important to have a small amplitude of spatial oscillations. To reach this, the lattice height must be large enough.

4.3. Measurement of potential of the forces using a condensate in a double-well trap

A new possibility of measurements of small potential differences is opened by an atomic interferometer with a Bose–Einstein condensate in a double-well potential [11]. In this experiment, a condensate containing over 10^5 atoms of ^{23}Na was trapped in a double-well optical trap. This trap was formed by a collimated laser beam that passed through an acousto-optic modulator and was focused onto the condensate with a lens (see figure 6(*a*)). The AOM was driven simultaneously by two radio frequency signals with frequencies f_1 and f_2. The separation between the potential wells was controlled by the frequency difference $|f - f_2|$. In this way, one can change the potential from single well (figure 6(*b*)) to double well (figure 6(*c*)). The thickness of each focused beam was 5 μm. A single isolated potential had depth $U_0 = 2\pi\hbar \times 5$ kHz, a radial trap frequency was 615 Hz and axial one 30 Hz. The chemical potential of atoms was $\mu = 2\pi\hbar \times 3$ kHz.

Condensate was initially loaded into a single-well trap. After holding the cloud for 15 s to damp oscillations of the condensate, the trap was deformed in double-well potential. Condensates realized from the double-well trap ballistically expanded, overlapped and

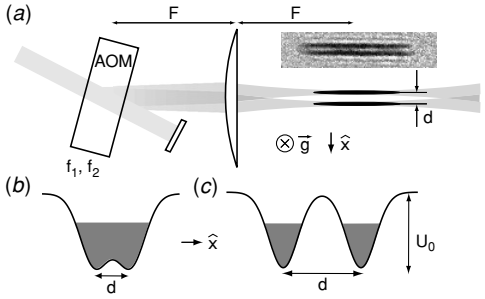

Figure 6. Atom interferometer with Bose–Einstein condensates. (*a*) Schematic diagram of the set-up and absorption image of two-well condensate. Energy diagrams for (*b*) initial single-well trap with $d = 6\,\mu$m and (*c*) final double-well trap with $d = 13\,\mu$m and potential 'dimple' $\sim 2\pi\hbar \times 500$ Hz. From [11].

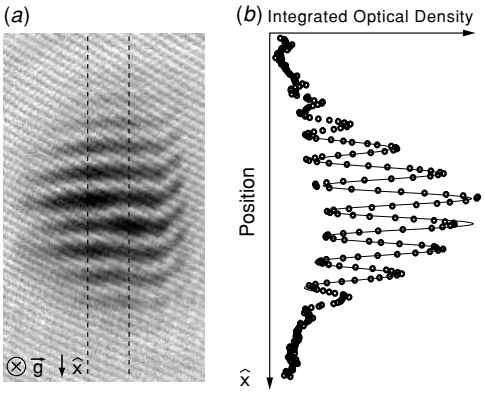

Figure 7. Interference of condensates released from the double-well potential in figure 6(*c*). (*a*) Absorption image of expanded condensates. (*b*) Radial density profile. From [11].

interfered (see figure 7). The relative phase between the two separated condensates was determined by the spatial phase of their interference pattern[4].

The possibility of the measurement of the potential difference with this interferometer is based on the Josephson equation for the time dependence of the phase of an individual condensate $\phi = -\mathrm{i}\mu t/\hbar$. If the condensates are placed in an external field with a potential $U(\boldsymbol{r})$ for a duration τ_p, they acquire a phase difference

$$\phi = -\mathrm{i}(\bar{U}_1 - \bar{U}_2)\tau_\mathrm{p}/\hbar \tag{34}$$

where $\bar{U}_1$ and $\bar{U}_2$ are the potentials averaged over volumes of condensates. In the experiment [11], the potential difference was created by pulsing off one of the wells for duration τ_p. To use this interferometer for the measurement of the Casimir forces, one of the wells must be moved to a small distance from a substrate surface [25]. After a duration τ_p, the condensate can be moved away from the substrate and the acquired phase difference can be measured.

[4] In the recent paper [26], authors developed a method of continuous non-destructive measurement of the relative phase. The method is based on the phenomenon of the 'interference in momentum space', predicted in [27]. The point is that the phase difference changes the momentum distribution of the two-well condensate. This distribution can be measured continuously by observation of stimulated two-photon scattering of light by the system.

However, practical realization of this idea demands a very high accuracy of the measurement of the relative phase.

Acknowledgments

New theoretical results presented in this paper have been obtained in collaboration with Mauro Antezza and Sandro Stringari. We are grateful to I Carusotto, E Cornell, C Eberlein, D M Harber, C Henkel, W Ketterle, J McGuirk, J Obrecht and S Reynaud for many useful comments. Financial support from MURST is acknowledged.

References

[1] Babb J F *et al* 2004 *Phys. Rev.* A **70** 042901
[2] Antezza M, Pitaevskii L P and Stringari S 2004 *Phys. Rev.* A **70** 053619
[3] Chan H B *et al* 2001 *Phys. Rev. Lett.* **87** 211801
[4] Dimopoulos S and Geraci A A 2003 *Phys. Rev.* D **68** 124021
[5] Decca R S *et al* 2005 *Ann. Phys., NY* **318** 37
[6] Sukenik C I *et al* 1993 *Phys. Rev. Lett.* **70** 560
[7] Landragin A *et al* 1996 *Phys. Rev. Lett.* **77** 1464
[8] Shimizu F 2001 *Phys. Rev. Lett.* **86** 987
[9] Oberst H *et al* 2005 *Phys. Rev.* A **71** 052901
[10] Lin Y J *et al* 2004 *Phys. Rev. Lett.* **92** 050404
[11] Pasquini T A *et al* 2004 *Phys. Rev. Lett.* **93** 223201
[12] Harber D M, Obrecht M, McGuirk J M and Cornell E A 2005 *Phys. Rev.* A **72** 033610
[13] Carusotto I *et al* 2005 *Phys. Rev. Lett.* **95** 093202
[14] Casimir H B G and Polder D 1948 *Phys. Rev.* **73** 360
[15] Dzyaloshinskii I E, Lifshitz E M and Pitaevskii L P 1961 *Adv. Phys.* **38** 165
[16] Lifshitz E M 1955 *Dokl. Akad. Nauk SSSR* **100** 879
[17] Henkel C, Joulain K, Mulet J-P and Greffet J-J 2002 *J. Opt. A: Pure Appl. Opt.* **4** S109
[18] Antezza M, Pitaevskii L P and Stringari S 2005 *Phys. Rev. Lett.* **95** 113202
[19] Rytov S M 1953 *Theory of Electric Fluctuations and Thermal Radiation* (Moscow: Academy of Sciences of USSR) (in Russian)
[20] Landau L D and Lifshitz E M 1960 *Electrodynamics of Continuous Media* (Oxford: Pergamon)
[21] Polder D and Van Hove M 1971 *Phys. Rev.* B **4** 3303
[22] Henkel C, Power B and Sols F 2005 *J. Phys.: Conf. Ser.* **19** 34
[23] Roati G *et al* 2004 *Phys. Rev. Lett.* **92** 230402
[24] Shin Y *et al* 2004 *Phys. Rev. Lett.* **92** 050405
[25] Ketterle W 2004 Private communication
[26] Saba M, Pasquini T A, Sanner C, Shin Y, Ketterle W and Pritchard D E 2005 *Science* **307** 1945
[27] Pitaevskii L P and Stringari S 1999 *Phys. Rev. Lett.* **83** 4237